SURFACE SUBDIVISION ALGORITHMS AND STRUCTURED LINEAR ALGEBRA: A COMPUTATIONAL APPROACH TO DETERMINE BOUNDS OF EXTRAORDINARY RULE WEIGHTS

MARCO DONATELLI[†], PAOLA NOVARA[†], LUCIA ROMANI[‡], STEFANO SERRA-CAPIZZANO[†,§], AND DEBORA SESANA[†]

Abstract. In the vicinity of extraordinary vertices, the action of a primal subdivision scheme for the construction of arbitrary topology surfaces can be represented by structured matrices that form a hybrid matrix algebra related to the block-circulant algebra. Exploiting the block diagonalization of such matrices, we can easily take into consideration the constraints to be satisfied by their eigenvalues and provide an efficient computational approach for determining the ranges of variability of the weights defining the extraordinary rules. Application examples of this computational strategy are shown to find the bounds of extraordinary rule weights for improved variants of two existing subdivision schemes.

Key words. Subdivision matrix; Block-circulant matrix algebra; Spectral decomposition; Extraordinary rule

AMS subject classifications. 65F15, 65F30, 65D17

1. State of the art and contributions of our work. Subdivision schemes are efficient iterative methods to generate arbitrary topology surfaces as the limit of a recursive process starting from a given polygonal mesh of arbitrary manifold topology. Primal subdivision schemes are the ones that, at each step of the recursive process, subdivide the faces of the given mesh to create a new mesh with more faces, edges and vertices than the original one. In particular, subdivision schemes of arity m split up each face into m^2 smaller faces, i.e. binary schemes subdivide each face into 4 smaller faces, while ternary schemes into 9 (see Figure 1).

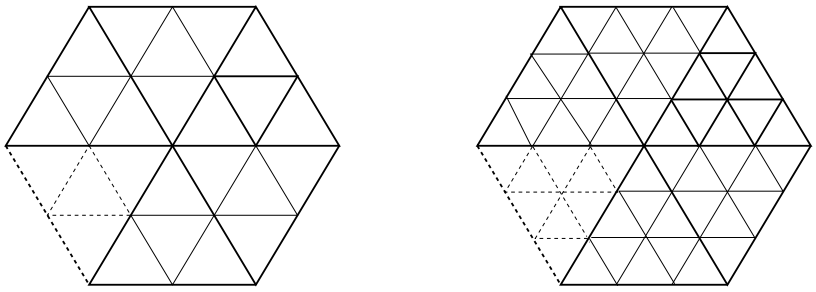

(a) Binary scheme ($m = 2$) (b) Ternary scheme ($m = 3$)

FIG. 1. *Face splitting obtained after applying one step of a primal binary (a) and ternary (b) subdivision scheme for triangular meshes.*

[†]Department of Science and High Technology, University of Insubria, Como 22100, Italy (marco.donatelli@uninsubria.it, paola.novara@uninsubria.it, stefano.serrac@uninsubria.it, debora.sesana@uninsubria.it).

[‡]Department of Mathematics and Applications, University of Milano-Bicocca, Milano 20125, Italy (lucia.romani@unimib.it).

[§]Division of Scientific Computing, Department of Information Technology, University of Uppsala, Uppsala Box 337, SE-751 05, Sweden (stefano.serra@it.uu.se).

The face splitting is achieved by creating the vertices of the finer mesh via the application of special rules that assume different forms depending if the new vertex will be located in correspondence to a vertex, an edge or a face of the coarser mesh. Such rules identify the subdivision scheme and are respectively encoded in the so-called *vertex-point*, *edge-point* and *face-point stencils*. For linear subdivision schemes, all the stencils consist in local linear combinations of the vertices of the coarser mesh and the weights of these linear combinations strictly depend on the local configuration of points. When the scheme is primal, the local configuration of points is given by a central vertex plus a certain number of vertices lying on rings with increasing radial distance from it. When the central vertex is the meeting point of N edges and N faces, it is said to have *valence* N. For triangular meshes, a vertex of valence $N = 6$ is called *regular*, while for quadrilateral meshes regular vertices are the ones having valence $N = 4$. Vertices that do not match the regular valence are called *extraordinary*. For linear subdivision schemes, a step of subdivision on the points $\mathbf{f}^k$ in the neighborhood of a vertex of valence N, is shortly written in the form

$$\mathbf{f}^{k+1} = S_N \mathbf{f}^k,$$

where S_N denotes the so-called *local subdivision matrix* associated with the vertex of valence N. Primal subdivision algorithms are characterized by local subdivision matrices S_N of size $(pN+1)\times(pN+1)$, exactly in view of the fact that their refinement rules involve the central vertex of valence N, and N sectors with p vertices each coming from the rings around it. In order to keep the matrix size as small as possible, we emphasize that it is convenient to derive the value of p considering the exact number of rings required by the subdivision rules. Precisely, for primal subdivision schemes defined by r-ring rules, the number p of points contained in each sector will be

$$p = \frac{r(r+1)}{2}, \tag{1.1}$$

in case of triangular meshes, and

$$p = r(r+1),$$

for quadrilateral meshes.
Moreover, it is of crucial importance to know that, having labeled both the old and the new vertices in a symmetric way around the central vertex, the structure of the matrix S_N changes depending on the ordering of the entries of the vectors $\mathbf{f}^k$ and $\mathbf{f}^{k+1}$. Precisely:

Order 1. ordering the vertices outwards from the central vertex, that is on successive rings with increasing radial distance, yields a matrix S_N that, discarded the first row and column, is a $p \times p$ block-matrix where each block, of size $N \times N$, is circulant;

Order 2. ordering the vertices outwards within each sector, before moving on to the next, and labeling compatibly within the sectors, gives a matrix S_N that, discarded the first row and column, is a $N \times N$ block-circulant matrix with blocks of size $p \times p$.

Doo and Sabin [7] were the first to show that many properties of the limit surface can be investigated by studying the eigenproperties of the matrix S_N. Depending

on the ordering of points that has been chosen, the following different methods have appeared in the literature to analyze the spectrum of S_N.

Method 1. Originally presented by Doo and Sabin [7] and successively exploited by Ball and Storry [2] and by Zorin [21], it applies a similarity transform to S_N given by the matrix $\left[\begin{array}{c|c} 1 & 0 \\ \hline 0 & I_p \otimes F_N \end{array}\right]$ with I_p denoting the identity matrix of size p and F_N the Fourier matrix $F_N = \frac{1}{\sqrt{N}}\left[\mathrm{e}^{-\frac{2\pi \mathrm{i} j\ell}{N}}\right]_{j,\ell=0}^{N-1}$. Then, once a matrix with diagonal blocks is obtained, a permutation is applied to finally reduce the local subdivision matrix into a block-diagonal matrix containing one block of size $(p+1)\times(p+1)$ and $N-1$ blocks each of size $p \times p$.

Method 2. Introduced by Peters and Reif [15], it artificially extends each block of size $p \times p$ by one row and one column such that the local subdivision matrix assumes a standard block-circulant structure, and then diagonalizes it by applying the block-Fourier matrix $F_N \otimes I_{p+1}$.

We observe that, from a computational viewpoint, Method 2 offers the advantage of requiring the spectral analysis of matrices whose size does not change with N. However, this method generates $N-1$ eigenvalues "in surplus", that are not necessary to investigate the properties of the subdivision scheme. Therefore, in this paper we will construct the subdivision matrix S_N ordering the points as explained in Order 2, but, following the strategy used in [19], we will study the eigenproperties of S_N by applying a block diagonalization via the unitary matrix

$$\tilde{F}_N = \left[\begin{array}{c|c} 1 & 0 \\ \hline 0 & F_N \otimes I_p \end{array}\right].$$

In this way, the block-diagonal matrix

$$\tilde{F}_N S_N \tilde{F}_N^* = \begin{bmatrix} \tilde{M}_0 & 0 & \cdots & \cdots & 0 \\ 0 & \hat{M}_1 & \ddots & & \vdots \\ \vdots & \ddots & \hat{M}_2 & \ddots & \vdots \\ \vdots & & \ddots & \ddots & 0 \\ 0 & \cdots & \cdots & 0 & \hat{M}_{N-1} \end{bmatrix}, \tag{1.2}$$

with one block $\tilde{M}_0$ of size $(p+1)\times(p+1)$ and $N-1$ blocks $\hat{M}_\nu$, $\nu = 1,\ldots,N-1$, of size $p \times p$, is directly obtained, so that the eigenproperties of S_N can be read from the spectrum of the N blocks.

This computational strategy is successively exploited in the second part of the paper to provide the ranges of variability of the weights defining the extraordinary rules of two primal, symmetric subdivision schemes for triangular meshes. The first one is a binary subdivision scheme characterized by a vertex-point rule involving $N+1$ points and one free parameter, and an edge-point rule involving $N+1$ points and $\left\lfloor \frac{N+1}{2} \right\rfloor$ free parameters; the second one is a ternary subdivision scheme characterized by a vertex-point rule involving $N+1$ points and one free parameter, an edge-point rule involving $N+1$ points and $\left\lfloor \frac{N+1}{2} \right\rfloor$ free parameters, and a face-point rule involving 6 points and no free parameters. For such schemes, we require the *convex hull property*, i.e. we demand that the limit surface is contained into the convex hull of the initial

control mesh, and we study which constraints have to be imposed on the free weights appearing in the subdivision rules such that the spectral conditions needed to attain

- *convergence* to a continuous limit surface of the sequence of control meshes generated by the subdivision scheme,
- *tangent plane continuity* of the limit surface at extraordinary vertices,
- *boundedness of curvature* of the limit surface at extraordinary vertices,
- *optimal shrinkage* of the local configuration of points around extraordinary vertices (thus ensuring that at each subdivision step the mesh edges are shortened by a factor of $\frac{1}{m}$),

are all simultaneously fulfilled. In particular, for both the schemes we focus our study on valences $N = 5$ and $N = 7$ since it has been proven that they are the only extraordinary vertices to be of crucial importance in case of triangle meshes. In fact, besides the fact that vertices with valence less than 5 or greater than 7 are problematic for many mesh processing tasks, surfaces of arbitrary manifold topology can be always obtained by using triangle meshes whose vertices have valences $N = 5, 6, 7$ only [1]. Very recently, it was also proposed a remeshing algorithm that locally retriangulates a mesh containing extraordinary vertices of any valence to obtain a mesh with only valences $N = 5, 6, 7$ [20]. Thus, thanks to this algorithm any arbitrary manifold topology mesh can be transformed into a 567-mesh.

To be more precise, the contents of our paper can be summarized as follows. In Section 2, we recall basic notions on block-circulant matrices and we introduce the so-called hybrid block-circulant algebra to have a convenient representation of local subdivision matrices. Section 3 contains a brief review of the spectral properties a subdivision matrix must necessarily have in order to define a subdivision scheme generating limit surfaces with particular characteristics. Section 4 illustrates how the block diagonalization of subdivision matrices via unitary transforms associated with the block-Fourier matrix can give rise to an efficient computational approach for determining the ranges of variability of the weights defining the extraordinary rules. In particular, application examples of this computational strategy are illustrated for improved variants of two existing subdivision schemes. Conclusions are drawn in Section 5.

2. Background knowledge on matrix algebras: block-circulant and hybrid block-circulant algebras. In this section we sketch the main properties of the famous block-circulant algebra, introducing then the so-called hybrid block-circulant algebra, useful for the spectral study of subdivision matrices of primal subdivision schemes. Block-circulants form an algebra and represent a subspace of block-Toeplitz used for their approximation in numerical methods such as multigrid methods, preconditioned Krylov methods and combination of them: for the algebraic properties of such algebra see [5]; for the numerical techniques related to these structures see [11]. In particular such matrices are encountered in signal/image processing (see the problem of signal reconstruction with missing data [6]), in Markov chain problems (see [4] and references therein), in the approximation of vector partial differential equations (PDEs) as the elasticity problem (see [8]), or of scalar PDEs by standard Finite Element methods [9]. To confirm their pervasive nature, these structures arise in the context of our approximation problems as described below.
A matrix A_N of size pN is called block-circulant if its entries $a_j \in \mathbb{C}^{p\times p}$, $j =$

$0, \ldots, N-1$, obey the rule $A_N = [a_{(s-r) \bmod N}]_{r,s=0}^{N-1}$, that is

$$A_N = \begin{bmatrix} a_0 & a_1 & \cdots & a_{N-2} & a_{N-1} \\ a_{N-1} & a_0 & a_1 & \ddots & a_{N-2} \\ a_{N-2} & a_{N-1} & \ddots & \ddots & \vdots \\ \vdots & \ddots & \ddots & \ddots & a_1 \\ a_1 & \cdots & a_{N-2} & a_{N-1} & a_0 \end{bmatrix}.$$

Thus, the following spectral decomposition holds

$$A_N = (F_N^* \otimes I_p) D_N (F_N \otimes I_p),$$

where $\otimes$ is the Kronecker product of matrices, F_N^* is the conjugate transpose of F_N, and

$$D_N = \operatorname{diag}(\sqrt{N} F_N^* \underline{a}),$$

is a block-diagonal matrix with $\underline{a} = [a_0, a_1, \ldots, a_{N-1}]^T$ denoting the first block-row of the matrix A_N.

REMARK 1. *Usually, the block-circulant matrix is defined with* $\underline{a} = [a_0, a_1, \ldots, a_{N-1}]$ *as the first block-column instead of the first block-row. Here we use this formulation to meet the notations used in the context of subdivision schemes.*

If we embed the block-circulant matrix A_N in a structure with this form

$$\tilde{A}_N = \left[\begin{array}{c|ccc} u & \mathbf{v}^T & \cdots & \mathbf{v}^T \\ \hline \mathbf{w} & & & \\ \vdots & & A_N & \\ \mathbf{w} & & & \end{array}\right],$$

with $u \in \mathbb{C}$ and $\mathbf{v}, \mathbf{w} \in \mathbb{C}^{p \times 1}$ so that $\tilde{A}_N \in \mathbb{C}^{(pN+1)\times(pN+1)}$, we can construct a new algebra of matrices, the so called hybrid block-circulant algebra, such that

$$\tilde{A}_N = \tilde{F}_N^* \tilde{D}_N \tilde{F}_N,$$

where

$$\tilde{F}_N = \left[\begin{array}{c|c} 1 & 0 \\ \hline 0 & F_N \otimes I_p \end{array}\right] \quad \text{and} \quad \tilde{D}_N = \left[\begin{array}{c|ccc} u & \sqrt{N}\mathbf{v}^T & 0 & 0 \\ \hline \sqrt{N}\mathbf{w} & & & \\ 0 & & D_N & \\ 0 & & & \end{array}\right].$$

3. Background knowledge on subdivision algorithms: spectral properties of the subdivision matrix and limit surface characteristics. Primal subdivision schemes are characterized by a local subdivision matrix $S_N \in \mathbb{R}^{(pN+1)\times(pN+1)}$ of the form

$$S_N = \left[\begin{array}{c|ccccc} a & \mathbf{b}^T & \mathbf{b}^T & \cdots & \mathbf{b}^T & \mathbf{b}^T \\ \hline \mathbf{c} & M_0 & M_1 & \cdots & M_{N-2} & M_{N-1} \\ \mathbf{c} & M_{N-1} & M_0 & M_1 & \ddots & M_{N-2} \\ \mathbf{c} & M_{N-2} & M_{N-1} & \ddots & \ddots & \vdots \\ \vdots & \vdots & \ddots & \ddots & \ddots & M_1 \\ \mathbf{c} & M_1 & \cdots & M_{N-2} & M_{N-1} & M_0 \end{array}\right], \tag{3.1}$$

where $a \in \mathbb{R}$, $\mathbf{b}, \mathbf{c} \in \mathbb{R}^{p\times 1}$ and $M_j \in \mathbb{R}^{p\times p}, j = 0, \dots, N-1$. The matrix S_N thus belongs to the hybrid block-circulant matrix algebra described in Section 2. As a consequence, it satisfies

$$\tilde{F}_N S_N \tilde{F}_N^* = \left[\begin{array}{c|ccccc} a & \sqrt{N}\mathbf{b}^T & 0 & \cdots & 0 & 0 \\ \hline \sqrt{N}\mathbf{c} & \hat{M}_0 & 0 & \cdots & 0 & 0 \\ 0 & 0 & \hat{M}_1 & 0 & \ddots & 0 \\ 0 & 0 & 0 & \ddots & \ddots & \vdots \\ \vdots & \vdots & \ddots & \ddots & \ddots & 0 \\ 0 & 0 & \cdots & 0 & 0 & \hat{M}_{N-1} \end{array}\right], \tag{3.2}$$

where the blocks $\hat{M}_\nu$, $\nu = 0, \dots, N-1$, are obtained by the blocks M_j, $j = 0, \dots, N-1$, applying a discrete Fourier transform

$$\hat{M}_\nu = \sum_{j=0}^{N-1} \omega^{j\nu} M_j, \qquad \nu = 0, 1, \dots, N-1,$$

where $\omega = e^{\mathrm{i}\frac{2\pi}{N}}$. Now, let

$$\tilde{M}_0 = \left[\begin{array}{cc} a & \sqrt{N}\mathbf{b}^T \\ \sqrt{N}\mathbf{c} & \hat{M}_0 \end{array}\right].$$

Thus, the matrix in (3.2) can be rewritten as in (1.2).
It is well-known that, to guarantee that the subdivision surface will lie within the convex hull of the control mesh, all the entries of S_N have to be in $[0, 1]$, i.e. all the weights appearing in the subdivision rules have to be in such interval.
Now, let λ_i, $i = 0, \dots, pN$, be the eigenvalues of the local subdivision matrix S_N sorted in decreasing order of their modulus.

Definition 1. *For any $\nu = 1, \dots, N-1$, if λ_i is an eigenvalue of $\hat{M}_\nu$ we call ν the Fourier index of λ_i and we write $\mathcal{F}(\lambda_i) = \nu$. If λ_i is an eigenvalue of $\tilde{M}_0$, we say that 0 is the Fourier index of λ_i and we write $\mathcal{F}(\lambda_i) = 0$.*

In order to attain a subdivision surface with certain characteristics, the local subdivision matrix S_N is required to fulfill specific spectral properties, that for the reader's convenience are recalled in the following (see, e.g., [7, 15, 16, 17, 22]):

(I) *Requirements for convergence:*
Unless $\lambda_0 = 1$ which must have Fourier index 0, all other eigenvalues of S_N have to be less than 1 in modulus, i.e.

$$1 = \lambda_0 > |\lambda_1|, \qquad \text{with} \quad \mathcal{F}(1) = 0.$$

(II) *Requirements for tangent plane continuity:*
The sub-dominant eigenvalue has to be double, equal to a real positive λ, with Fourier indices $1, N-1$, and all other eigenvalues have to be less than λ in modulus, i.e.

$$1 = \lambda_0 > \lambda := \lambda_1 = \lambda_2 > |\lambda_3|, \quad \lambda \in \mathbb{R}^+, \quad \mathcal{F}(\lambda) = \{1,\, N-1\}.$$

(III) *Requirements for boundedness of curvature:*
The subsub-dominant eigenvalue has to be triple, equal to λ^2, with Fourier indices $0, 2, N-2$, and all other eigenvalues have to be not larger than λ^2 in modulus, i.e.

$$1 = \lambda_0 > \lambda := \lambda_1 = \lambda_2 > \mu := \lambda_3 = \lambda_4 = \lambda_5 \geq |\lambda_6|, \quad \mathcal{F}(\mu) = \{0,\, 2,\, N-2\}.$$

(IV) *Requirements for optimal shrinkage:*
The sub-dominant eigenvalue λ has to be equal to $\frac{1}{m}$ (or the closest possible to $\frac{1}{m}$), where m is the arity of the subdivision scheme.

Now, for any $\nu = 1, \ldots, N-1$, let λ_r^ν be the r-th eigenvalue of $\hat{M}_\nu$ and let λ_r^0 be the r-th eigenvalue of $\tilde{M}_0$. In this way, properties (I)-(IV) can be rewritten as in Table 1.

Regarding the property (IV), the sub-dominant eigenvalue λ defines the shrinking factor by which the size of the local configuration is scaled in every subdivision step. In the optimal setting, the value for λ equals the shortening factor of the edges caused by the refinement operator, e.g. $\lambda = \frac{1}{2}$ for binary subdivision and $\lambda = \frac{1}{3}$ for ternary subdivision. If the actual λ happens to deviate significantly from that optimal value, the face shrinkage near extraordinary vertices is much faster or much slower than elsewhere which leads to the so-called polar artifacts [3, 18].

Note that for subdivision schemes on triangular meshes it makes sense to consider only the cases of valence $N \geq 5, N \neq 6$, because for $N = 3, 4$ we might not have enough eigenvalues to satisfy all the properties. In fact, if S_N is the subdivision matrix of a 1-ring scheme for triangular meshes, then from (1.1) it is defined by N blocks M_i, $i = 0, \ldots, N-1$, of size 1×1. Thus we could have only 4 eigenvalues when $N = 3$ and 5 when $N = 4$. There follows that in these cases, we are not able to obtain condition (III) (see also [13]). On the other hand, properties of the limit surface in the regular case $N = 6$ are usually studied in a different way which does not involve the analysis of the eigenproperties of S_N (see, e.g., [12, 15]).

Conditions to be satisfied by the eigenvalues of S_N
(i) $\lambda_0^0 = 1$, $\lambda_1^0 = \lambda^2$
(ii) $\lambda_0^1 = \lambda$, $\lambda_0^{N-1} = \lambda$
(iii) $\lambda_0^2 = \lambda^2$, $\lambda_0^{N-2} = \lambda^2$
(iv) the modulus of all the other eigenvalues is not larger than λ^2
(v) $\lambda = \frac{1}{m}$ (m = arity of the subdivision scheme).

TABLE 1
Conditions to be satisfied by the eigenvalues of S_N.

REMARK 2. *The conditions summarized in Table 1 are not sufficient to guarantee the generation of C^1 continuous limit surfaces. In fact, they do not take into account the behavior of the characteristic map, that is the surface determined by the pair of subdominant eigenvectors associated to λ. Additionally requiring that this map is regular and injective, we can indeed guarantee that the limit surface produced by the subdivision scheme will be C^1 with bounded curvature, convex hull property and optimal shrinkage [15]. However, as also previously done in [10, 13], in this manuscript we focus our attention on the spectral properties of the subdivision matrix that are essential to obtain C^1 limit surfaces with bounded curvature, convex hull property and optimal shrinkage effect.*

4. Computing bounds for extraordinary rule weights. Exploiting all the notions recalled in the previous sections, we now define a computational strategy to find the weights of extraordinary stencils in order to obtain limit surfaces with the desired characteristics. In practice, we start by considering refinement rules of a primal subdivision scheme which depend on some free parameters. From these rules, we construct the subdivision matrix S_N as in (3.1) and, using the discrete Fourier transform, we obtain a similar block-diagonal matrix as in (3.2). We compute the eigenvalues of each block and, taking into consideration Definition 1, we impose on them the necessary conditions for convergence, tangent plane continuity and boundedness of curvature summarized in Table 1. In the above conditions we set $\lambda = \frac{1}{m}$ to guarantee also the optimal shrinkage. These computations allow us to find the ranges in which the free parameters defining the subdivision rules could vary. Finally, to ensure also the convex hull property, we require that the range of variability of each parameter is contained in $[0, 1]$. In the following, we apply these general strategy to two examples of primal subdivision schemes for triangular meshes, both improving the well-known Loop's subdivision scheme [12].

4.1. Loop's scheme. In 1987 C. Loop proposed a binary subdivision scheme for triangular meshes, capable of producing a limit surface that is C^2 continuous everywhere except at the extraordinary points where it is only C^1. Although Loop's limit surface satisfies the convex hull property, neither boundedness of curvature nor optimal shrinkage are achieved [12]. The vertex-point and edge-point stencils of this scheme are shown in Figure 2, and the corresponding subdivision rules read as

$$\begin{aligned} V &= \delta P_0 + \sum_{i=1}^{N} \left(\frac{1-\delta}{N} P_i \right), \qquad \delta = \left(\frac{3}{8} + \frac{1}{4} \cos\left(\frac{2\pi}{N} \right) \right)^2 + \frac{3}{8}, \\ E &= \frac{3}{8}(P_0 + P_1) + \frac{1}{8}(P_2 + P_N), \end{aligned} \tag{4.1}$$

where P_0 denotes the central (extraordinary) vertex, P_1 the vertex on its right hand side and P_i, $i = 2, \ldots, N$ all the remaining ones ordered counterclockwise. We notice that while the vertex-point rule depends on the valence N of the extraordinary vertex, the edge-point rule is not influenced by N.
During the years different improvements of original Loop's subdivision scheme have been proposed to gain boundedness of curvature at extraordinary vertices. The goal has been reached by considering either a larger edge-point stencil [10, 13] or a suitable transformation of the subdivision rules into the ternary setting [14]. The resulting innovative schemes in [13, 14] propose vertex-point and edge-point stencils where the weights assume a specific appropriate value in order to produce a limit surface of class C^1 and with bounded curvature at extraordinary vertices. However, the property of optimal shrinkage is never reached except for the regular case $N = 6$. The goal of this section is to consider the stencils of modified binary Loop's scheme as well as of ternary Loop's scheme, and to apply our theoretical results in order to determine in which ranges the stencil weights could vary to achieve not only the boundedness of curvature and the convex hull property, but also the optimal shrinkage property at extraordinary vertices of valence $N \geq 5, N \neq 6$.

4.2. Binary Loop's scheme: 1-ring rules. In [13], new rules of binary Loop's scheme near an extraordinary vertex of valence $N \neq 6$ have been proposed, which are described by the stencils in Figure 3. The coefficients δ, α, β_j, $j = 0, \ldots, N-1$ chosen by the author satisfy the properties of convex hull, tangent plane continuity and

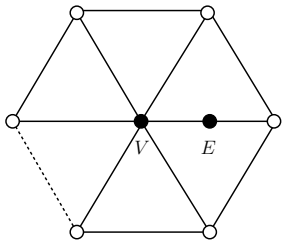

(a) Original Loop's scheme

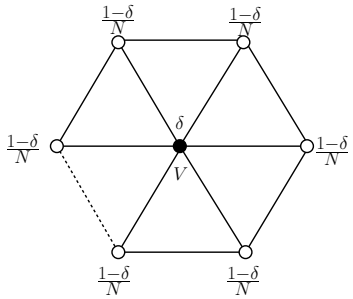

(b) Original Loop's vertex-point stencil

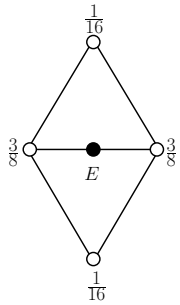

(c) Original Loop's edge-point stencil

FIG. 2. *Vertex-point stencil and edge-point stencil of original Loop's subdivision scheme in the case of vertices of valence N.*

boundedness of curvature at extraordinary vertices, but not the optimal shrinkage, i.e. the version of Loop's scheme in [13] satisfies requirements (i)-(iv) of Table 1, but not condition (v).

Comparing the extraordinary stencils of the bounded curvature version of Loop's scheme in Figure 3 with the original ones in Figure 2, we notice that the vertex-point rule has the same structure, while the edge-point rule of the new version of Loop's scheme involves a higher number of points than the original one and depends on the valence of the extraordinary vertex. Moreover, we notice that binary Loop's scheme is a 1-ring scheme, since both the vertex-rule and the edge-rule require just the contribution of the points that are on the first ring around the extraordinary vertex. In the following, we show the main steps to find new weights for the extraordinary stencils in Figure 3 in order to satisfy not only the properties of convex hull, tangent plane continuity and boundedness of curvature, but also optimal shrinkage. Since we have a binary scheme, the arity is $m = 2$, so condition (v) is satisfied by setting $\lambda = \frac{1}{2}$. First of all, we notice that for the symmetry of the scheme we have

$$\beta_j = \beta_{N-j}, \quad j = 1, \ldots, N-1, \tag{4.2}$$

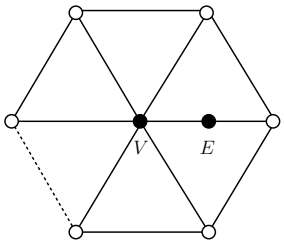

(a) New Loop's scheme

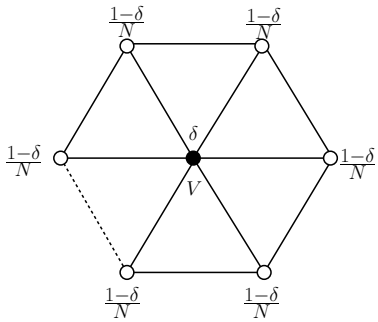

(b) New Loop's vertex-point stencil

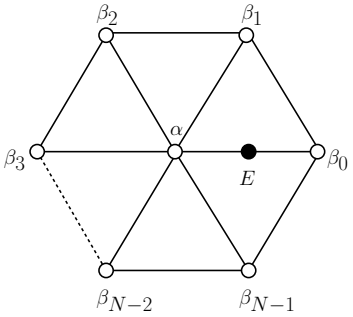

(c) New Loop's edge-point stencil

Fig. 3. *Stencils for the vertex-point rule and the edge-point rule of new Loop's subdivision scheme at vertices of valence N.*

and

(4.3)
$$\beta_{\lfloor \frac{N}{2} \rfloor} = \begin{cases} \dfrac{1}{2}\left(1-\alpha-\beta_0-2\displaystyle\sum_{j=1}^{\lfloor \frac{N}{2} \rfloor -1}\beta_j\right), & \text{if } N \text{ odd}, \\ 1-\alpha-\beta_0-2\displaystyle\sum_{j=1}^{\frac{N}{2}-1}\beta_j, & \text{if } N \text{ even}, \end{cases} \quad \Rightarrow \quad \sum_{j=0}^{N-1}\beta_j = 1-\alpha.$$

Then, we construct the subdivision matrix S_N with blocks $M_i \in \mathbb{R}^{p\times p}$, $i = 0, \ldots, N-1$. Since Loop's scheme has 1-ring rules, from (1.1) we simply have $p = 1$. Thus S_N is a hybrid circulant matrix of the form

$$S_N = \left[\begin{array}{c|cccccc} \delta & \frac{1-\delta}{N} & \frac{1-\delta}{N} & \cdots & \frac{1-\delta}{N} & \frac{1-\delta}{N} \\ \hline \alpha & \beta_0 & \beta_1 & \cdots & \beta_{N-2} & \beta_{N-1} \\ \alpha & \beta_{N-1} & \beta_0 & \beta_1 & \ddots & \beta_{N-2} \\ \alpha & \beta_{N-2} & \beta_{N-1} & \ddots & \ddots & \vdots \\ \vdots & \vdots & \ddots & \ddots & \ddots & \beta_1 \\ \alpha & \beta_1 & \cdots & \beta_{N-2} & \beta_{N-1} & \beta_0 \end{array}\right].$$

Then, we apply the discrete Fourier transform obtaining

$$\hat{M}_\nu = \sum_{j=0}^{N-1} \beta_j \omega^{j\nu}, \quad \nu = 1, \dots, N-1, \qquad \text{and} \qquad \tilde{M}_0 = \begin{pmatrix} \delta & \frac{1-\delta}{\sqrt{N}} \\ \sqrt{N}\alpha & \sum_{j=0}^{N-1} \beta_j \end{pmatrix}. \tag{4.4}$$

Since $p = 1$ we have $\hat{M}_\nu = \lambda_0^\nu$ and, in particular,

$$\lambda_0^\nu = \sum_{j=0}^{N-1} \beta_j \omega^{j\nu}, \quad \nu = 1, \dots, N-1, \tag{4.5}$$

while for $\tilde{M}_0$, thanks to (4.3), we find $\lambda_0^0 = 1$, $\lambda_1^0 = \delta - \alpha$.

Remark 3. *Since for $j = 1, \dots, N-1$ we have $\omega^{j\nu} + \omega^{(N-j)\nu} = \omega^{j(N-\nu)} + \omega^{(N-j)(N-\nu)}$ and, for N even, $\omega^{\frac{N}{2}\nu} = \omega^{\frac{N}{2}(N-\nu)}$, from (4.2) and (4.5) it holds*

$$\lambda_0^\nu = \lambda_0^{N-\nu},$$

so conditions (ii)-(iii) of Table 1 reduce to $\lambda_0^1 = \lambda$ and $\lambda_0^2 = \lambda^2$, respectively.

Summarizing, taking into account Remark 3, the condition (i) in Table 1 is satisfied with

$$\delta - \alpha = \frac{1}{4}, \tag{4.6}$$

the condition (ii) leads to

$$\sum_{j=0}^{N-1} \beta_j \omega^j = \frac{1}{2}, \tag{4.7}$$

and from condition (iii) has to hold

$$\sum_{j=0}^{N-1} \beta_j \omega^{2j} = \frac{1}{4}. \tag{4.8}$$

Finally, to gain also condition (iv), we have to check for which ranges of the free parameters we have $|\lambda_0^\nu| \leq \frac{1}{4}$, for $\nu = 3, \dots, N-3$, and if the convex hull property is satisfied, i.e. all the free parameters are in $[0, 1]$.

Remark 4. *From (4.6) it is clear that α and δ are strictly related. If we find an expression for α, then $\delta = \frac{1}{4} + \alpha$ and, in order to ensure the convex hull property also for δ, we have to restrict the set of values for α to $\left[0, \frac{3}{4}\right]$. On the other hand, if we obtain δ, then $\alpha = \delta - \frac{1}{4}$ with $\delta \in \left[\frac{1}{4}, 1\right]$ for the convex hull property for α.*

In the following, we show the details of the computation for the cases $N = 5$ and $N = 7$ since, as already recalled in Section 1, these are considered the only crucial extraordinary valences when dealing with triangular meshes.

Proposition 4.1. *Binary Loop's scheme with extraordinary stencils in Figure 3 satisfies the conditions (I)-(IV) and the convex hull property at an extraordinary vertex of valence $N = 5$ if*

$$\beta_1 \in \left[\frac{\sqrt{5}}{20}, \frac{\sqrt{5}+5}{40}\right] \approx [0.1118, 0.1809], \tag{4.9}$$

and

$$\alpha = \frac{\sqrt{5}+5}{8} - 5\beta_1, \quad \beta_0 = \beta_1 + \frac{15-\sqrt{5}}{40}, \quad \beta_2 = \beta_1 - \frac{\sqrt{5}}{20}, \quad \delta = \frac{\sqrt{5}+7}{8} - 5\beta_1,$$

with $\beta_3 = \beta_2$ *and* $\beta_4 = \beta_1$.

Proof. In case of extraordinary vertex of valence $N = 5$, recalling the condition (4.2), the stencil weights are $\alpha, \beta_0, \beta_1, \beta_2$ and δ with

$$\beta_2 = \frac{1}{2}(1 - \alpha - \beta_0 - 2\beta_1), \tag{4.10}$$

thanks to (4.3). For $N = 5$, the expressions in (4.4) become

$$\hat{M}_\nu = \beta_0 + \beta_1(\omega^\nu + \omega^{4\nu}) + \beta_2(\omega^{2\nu} + \omega^{3\nu}) \qquad \text{and} \qquad \tilde{M}_0 = \begin{pmatrix} \delta & \frac{1-\delta}{\sqrt{5}} \\ \sqrt{5}\alpha & 1-\alpha \end{pmatrix},$$

since $\sum_{j=0}^{4} \beta_j = 1 - \alpha$. Hence, from (4.7) and (4.10), we have

$$\begin{aligned} \frac{1}{2} &= \beta_0 + \beta_1(\omega + \omega^4) + \beta_2(\omega^2 + \omega^3) \\ &= \frac{1}{2}(\omega^2 + \omega^3) - \frac{\alpha}{2}(\omega^2 + \omega^3) + \beta_0(1 - \frac{1}{2}(\omega^2 + \omega^3)) + \beta_1(\omega + \omega^4 - (\omega^2 + \omega^3)) \\ &= -\frac{\sqrt{5}+1}{4} + \frac{\sqrt{5}+1}{4}\alpha + \frac{\sqrt{5}+5}{4}\beta_0 + \sqrt{5}\beta_1, \end{aligned}$$

where the last equality holds for $\omega + \omega^4 = \frac{\sqrt{5}-1}{2}$ and $\omega^2 + \omega^3 = -\frac{\sqrt{5}+1}{2}$. Similarly, it holds

$$\frac{\sqrt{5}-1}{4} - \frac{\sqrt{5}-1}{4}\alpha + \frac{5-\sqrt{5}}{4}\beta_0 - \sqrt{5}\beta_1 = \frac{1}{4},$$

thanks to equation (4.8). From these relations, we find

$$\alpha = \frac{\sqrt{5}+5}{8} - 5\beta_1, \qquad \beta_0 = \beta_1 + \frac{15-\sqrt{5}}{40},$$

and, as a consequence of (4.10), $\beta_2 = \beta_1 - \frac{\sqrt{5}}{20}$. Moreover, (4.6) gives $\delta = \frac{\sqrt{5}+7}{8} - 5\beta_1$, and since there are no other eigenvalues, condition (iv) in Table 1 is verified too. Now we have to ensure the convex hull property for all the parameters, that is, by considering Remark 4,

$$\begin{aligned} \alpha \in \left[0, \frac{3}{4}\right] \qquad &\Leftrightarrow \qquad \beta_1 \in \left[\frac{\sqrt{5}-1}{40}, \frac{\sqrt{5}+5}{40}\right] \approx [0.0309, 0.1809], \\ \beta_0 \in [0,1] \qquad &\Leftrightarrow \qquad \beta_1 \in \left[\frac{\sqrt{5}-15}{40}, \frac{\sqrt{5}+25}{40}\right] \approx [-0.3191, 0.6809], \\ \beta_2 \in [0,1] \qquad &\Leftrightarrow \qquad \beta_1 \in \left[\frac{\sqrt{5}}{20}, \frac{\sqrt{5}+20}{20}\right] \approx [0.1118, 1.1118], \end{aligned}$$

and the intersection of these intervals (taking into account, if necessary, that also β_1 should be in $[0,1]$) gives (4.9). ∎

PROPOSITION 4.2. *Binary Loop's scheme with extraordinary stencils in Figure 3 satisfies the conditions (I)-(IV) and the convex hull property at an extraordinary vertex of valence $N=7$ if, setting $c_j = 2\cos\frac{j\pi}{7}$, $j=2,4,6$,*

(4.11)
$$\beta_1 \in \left[\frac{4+c_2+c_4-2c_2c_6}{28c_2+8c_4-36c_6+8c_2c_4-8c_4c_6}, \frac{36+33c_2+10c_4-31c_6+6c_2c_4-20c_2c_6-7c_4c_6+3c_2c_4c_6}{196c_2+20c_4-216c_6+20c_2c_4-20c_4c_6}\right] \approx [0.1089, 0.2804],$$

(4.12)
$$\beta_2 \in \left[\max\left\{\frac{1+4(c_4-c_2)\beta_1}{4(c_4-c_6)}, 0, \frac{3c_2-c_4-2c_6}{4(c_2c_6+c_2c_4-6-c_4-c_6-c_2+c_4c_6)}+\beta_1\right\}, \min\left\{\frac{c_2-c_4}{4(c_2c_6+c_2c_4-6-c_4-c_6-c_2+c_4c_6)}+\beta_1, \frac{2+2c_2-3c_6+4(2-4c_2+3c_4+2c_6-c_4c_6)\beta_1}{4(2+3c_2+2c_4-4c_6-c_2c_4)}\right\}\right],$$

and

$$\alpha = \frac{1}{4(c_2-c_6)}\left[2+2c_2-3c_6+4(2-4c_2+3c_4+2c_6-c_4c_6)\beta_1+ +4(-2-3c_2-2c_4+4c_6+c_2c_4)\beta_2\right], \tag{4.13}$$

$$\beta_0 = \frac{1}{4(c_2-c_6)}\left[2c_2-c_6+4(-2-c_4+c_4c_6)\beta_1+4(2+c_2-c_2c_4)\beta_2\right], \tag{4.14}$$

$$\beta_3 = \frac{1}{4(c_2-c_6)}\left[-1+4(c_2-c_4)\beta_1+4(c_4-c_6)\beta_2\right], \tag{4.15}$$

$$\delta = \frac{1}{4(c_2-c_6)}\left[2+3c_2-4c_6+4(2-4c_2+3c_4+2c_6-c_4c_6)\beta_1+ +4(-2-3c_2-2c_4+4c_6+c_2c_4)\beta_2\right], \tag{4.16}$$

with $\beta_4=\beta_3$, $\beta_5=\beta_2$ and $\beta_6=\beta_1$.

Proof. Following the same reasoning of the previous proof, in case of an extraordinary vertex of valence $N=7$, the stencil weights are $\alpha, \beta_0, \beta_1, \beta_2, \beta_3$ and δ with

$$\beta_3 = \frac{1}{2}(1-\alpha-\beta_0-2\beta_1-2\beta_2). \tag{4.17}$$

If $N=7$, the formulas in (4.4) become

$$\hat{M}_\nu = \beta_0+\beta_1(\omega^\nu+\omega^{6\nu})+\beta_2(\omega^{2\nu}+\omega^{5\nu})+\beta_3(\omega^{3\nu}+\omega^{4\nu}),$$

and

$$\tilde{M}_0 = \begin{pmatrix} \delta & \frac{1-\delta}{\sqrt{7}} \\ \sqrt{7}\alpha & 1-\alpha \end{pmatrix}.$$

From (4.7) and (4.8), exploiting (4.17), we have

$$\begin{aligned} -\frac{1}{2}c_6\alpha+\left(1-\frac{1}{2}c_6\right)\beta_0+(c_2-c_6)\beta_1+(c_4-c_6)\beta_2+\frac{1}{2}c_6 &= \frac{1}{2}, \\ -\frac{1}{2}c_2\alpha+\left(1-\frac{1}{2}c_2\right)\beta_0+(c_4-c_2)\beta_1+(c_6-c_2)\beta_2+\frac{1}{2}c_2 &= \frac{1}{4}. \end{aligned}$$

These equations give α and β_0 as in (4.13)-(4.14), and we obtain β_3 and δ in (4.15)-(4.16) as a consequence of (4.17) and (4.6), respectively. Moreover, from condition (iv) in Table 1, we require $|\lambda_0^3|, |\lambda_0^4| \leq \frac{1}{4}$. Since Remark 3 ensures that $\lambda_0^3 = \lambda_0^4$, the previous inequality is verified from (4.5) with $\nu = 3$ if

$$-\frac{1}{4} \leq \frac{4(c_2c_6 + c_2c_4 - 6 - c_4 - c_6 + c_4c_6 - c_2)(\beta_1 - \beta_2) + 2c_2 - c_6 - c_4}{4(c_2 - c_6)} \leq \frac{1}{4},$$

that is

$$\lambda_0^3 \in \left[-\frac{1}{4}, \frac{1}{4}\right] \quad \Leftrightarrow \quad \beta_2 \in \frac{[3c_2 - c_4 - 2c_6, c_2 - c_4]}{4(c_2c_6 + c_2c_4 - 6 - c_4 - c_6 - c_2 + c_4c_6)} + \beta_1. \tag{4.18}$$

Now we check the convex hull property, by remembering Remark 4,

(4.19)

$$\alpha \in \left[0, \frac{3}{4}\right] \quad \Leftrightarrow \quad \beta_2 \in \frac{[2 - c_2, 2 + 2c_2 - 3c_6] + 4(2 - 4c_2 + 3c_4 + 2c_6 - c_4c_6)\beta_1}{4(2 + 3c_2 + 2c_4 - 4c_6 - c_2c_4)},$$

$$\beta_0 \in [0, 1] \quad \Leftrightarrow \quad \beta_2 \in \frac{[2c_2 - c_6, -2c_2 + 3c_6] + 4(-2 - c_4 + c_4c_6)\beta_1}{4(c_2c_4 - 2 - c_2)},$$

$$\beta_3 \in [0, 1] \quad \Leftrightarrow \quad \beta_2 \in \frac{[1, 1 + 4c_2 - 4c_6] + 4(c_4 - c_2)\beta_1}{4(c_4 - c_6)}.$$

We observe that all the eligible values for β_2 in (4.19) and (4.18), for $\beta_1 \in [0, 1]$, are contained in regions of the plane delimited by two parallel lines (see Figure 4). The intersection of such regions, taking into account that also β_2 should be in $[0, 1]$ and using the notation explained in the caption of Figure 4, gives rise to

$$\beta_1 \in [(\beta_3)_{\mathrm{L}} \cap (\lambda_0^3)_{\mathrm{R}}, (\lambda_0^3)_{\mathrm{L}} \cap (\alpha)_{\mathrm{R}}],$$
$$\beta_2 \in [\max\{(\beta_3)_{\mathrm{L}}, 0, (\lambda_0^3)_{\mathrm{L}}\}, \min\{(\lambda_0^3)_{\mathrm{R}}, (\alpha)_{\mathrm{R}}\}],$$

which are written in full in (4.11) and (4.12). □

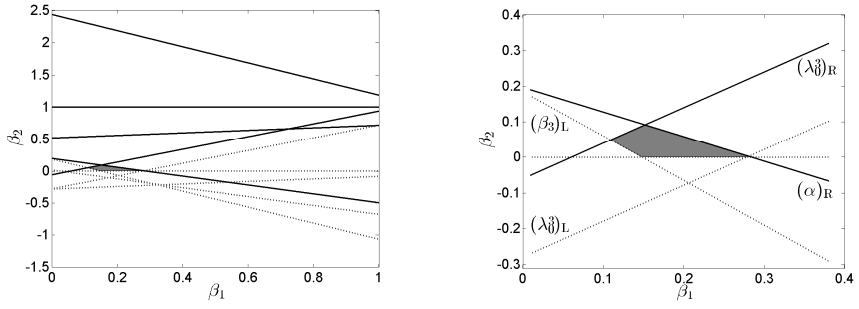

(a) (b)

Fig. 4. (a): $(\cdots)$ *lines demarcating the eligible regions from left,* $(-)$ *lines demarcating the eligible regions from right for* β_2*, given in (4.19) and (4.18), with* $\beta_1 \in [0, 1]$*: in gray is depicted the intersection of such eligible regions.* (b) *Zoom of the eligibility region in* (a) *with indications about the involved lines:* $(\theta)_{\mathrm{L}}$ *and* $(\theta)_{\mathrm{R}}$ *are, respectively, the left and the right demarcating lines of the regions of values for* β_2 *related to* $\theta \in \{\alpha, \beta_3, \lambda_0^3\}$*.*

Figure 5 illustrates the result of the new Loop's subdivision scheme when applied to triangle meshes containing only extraordinary vertices of valence $N = 5$ and $N = 7$ (initial data are courtesy of the authors of [1]). The free β parameters have been set accordingly to the identified bounds.

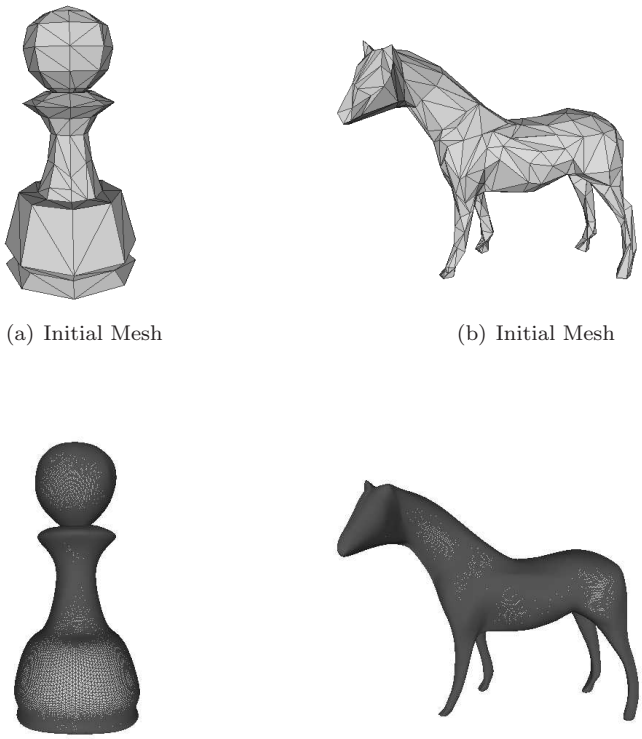

(a) Initial Mesh (b) Initial Mesh

(c) Refined Mesh (4 steps) (d) Refined Mesh (4 steps)

FIG. 5. *Refined meshes obtained from a* 567*-mesh using new binary Loop's scheme with parameters* $\beta_1 = 0.112$ *for* $N = 5$, $\beta_1 = 0.14, \beta_2 = 0.02$ *for* $N = 7$ *(left column) and* $\beta_1 = 0.13$ *for* $N = 5$, $\beta_1 = 0.16, \beta_2 = 0.022$ *for* $N = 7$ *(right column).*

4.3. Ternary Loop's scheme: 2-ring rules. To gain the boundedness of curvature in the limit surface, another possible modification of original Loop's scheme is its ternary version, proposed in [14], whose stencils are shown in Figure 6. We notice that, if in the binary case the scheme is defined by 2 stencils, one for the vertex-point and one for the edge-point, the ternary variant needs 3 different stencils to define the vertex-point, the edge-point and the face-point, respectively. In the regular case, $N = 6$, the stencil weights are

$$\alpha = \frac{2}{3}, \quad \beta_0 = \frac{20}{81}, \quad \beta_1 = \beta_5 = \frac{10}{81}, \quad \beta_2 = \beta_4 = \frac{2}{81}, \quad \beta_3 = \frac{1}{81}, \quad \delta = \frac{5}{9},$$

while near extraordinary vertices the coefficients proposed in [14] are chosen to satisfy conditions (i)-(iv) in Table 1 and the convex hull property, but not requirement (v) regarding the optimal shrinkage effect.
We notice that ternary Loop's scheme is a 2-ring scheme, since the vertex-point rule and the edge-point rule require just the contribution of the points on the first ring around the extraordinary vertex, but the face-point rule involves also the points of the second ring.
In the following, we apply the discussed computational strategy to find new weights

for the extraordinary stencils in Figure 6 in order to satisfy both the convex hull property and all requirements (i)-(v) in Table 1: since we have a ternary scheme, i.e. the arity is $m = 3$, condition (v) is satisfied by setting $\lambda = \frac{1}{3}$.

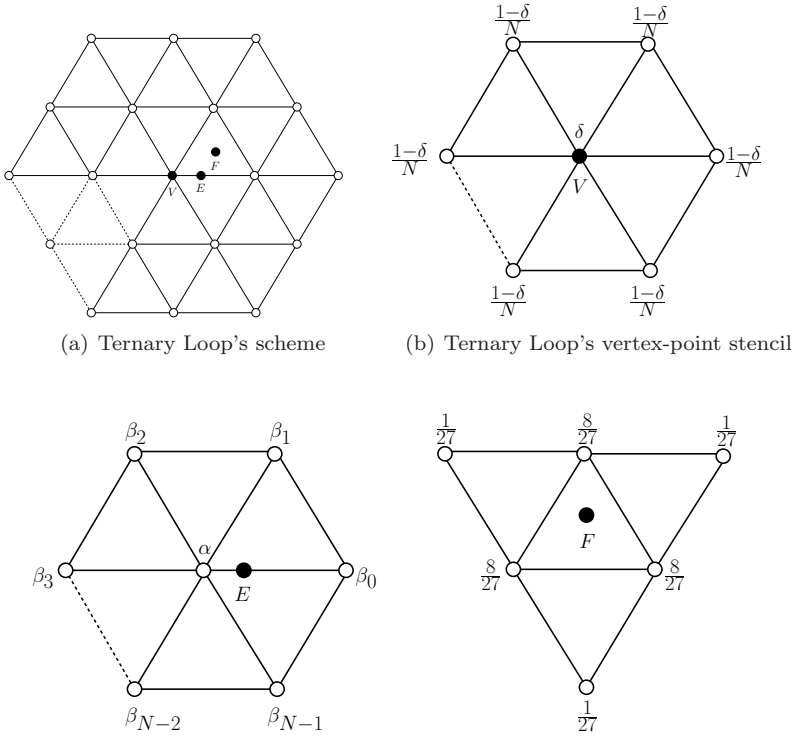

(a) Ternary Loop's scheme (b) Ternary Loop's vertex-point stencil

(c) Ternary Loop's edge-point stencil (d) Ternary Loop's face-point stencil

Fig. 6. *Stencils for the vertex-point rule, the edge-point rule and the face-point rule of ternary Loop's subdivision scheme at vertices of valence N.*

First of all, for the symmetry of the scheme, we require (4.2) and (4.3). Then, we start by constructing the subdivision matrix S_N with blocks $M_i \in \mathbb{R}^{p\times p}$, $i = 0, \ldots, N-1$. Since ternary Loop's scheme has 2-ring rules, from (1.1) we have $p = 3$. Thus S_N is a block-circulant matrix as in (3.1) with $a = \delta$, $\mathbf{b} = \left[\frac{1-\delta}{N}, 0, 0\right]^T$, $\mathbf{c} = \left[\alpha, \frac{20}{81}, \frac{8}{27}\right]^T$, and

$$M_0 = \begin{pmatrix} \beta_0 & 0 & 0 \\ \frac{4}{9} & \frac{1}{81} & \frac{2}{81} \\ \frac{8}{27} & 0 & \frac{1}{27} \end{pmatrix}, \qquad M_1 = \begin{pmatrix} \beta_1 & 0 & 0 \\ \frac{10}{81} & 0 & 0 \\ \frac{8}{27} & 0 & 0 \end{pmatrix}, \quad M_2 = \begin{pmatrix} \beta_2 & 0 & 0 \\ 0 & 0 & 0 \\ \frac{1}{27} & 0 & 0 \end{pmatrix},$$

$$M_i = \begin{pmatrix} \beta_i & 0 & 0 \\ 0 & 0 & 0 \\ 0 & 0 & 0 \end{pmatrix}, \ i = 3, \ldots, N-2, \qquad M_{N-1} = \begin{pmatrix} \beta_{N-1} & 0 & 0 \\ \frac{10}{81} & 0 & \frac{2}{81} \\ \frac{1}{27} & 0 & 0 \end{pmatrix}.$$

After applying the discrete Fourier transform we get

$$\hat{M}_\nu = \begin{pmatrix} \sum_{j=0}^{N-1} \beta_j \omega^{j\nu} & 0 & 0 \\ \frac{4}{9} + \frac{10}{81}(\omega^\nu + \omega^{(N-1)\nu}) & \frac{1}{81} & \frac{2}{81}(1+\omega^{(N-1)\nu}) \\ \frac{8}{27}(1+\omega^\nu) + \frac{1}{27}(\omega^{2\nu} + \omega^{(N-1)\nu}) & 0 & \frac{1}{27} \end{pmatrix}, \quad \nu = 1, \ldots, N-1,$$

and

$$\tilde{M}_0 = \begin{pmatrix} \delta & \frac{1-\delta}{\sqrt{N}} & 0 & 0 \\ \sqrt{N}\alpha & \sum_{j=0}^{N-1} \beta_j & 0 & 0 \\ \sqrt{N}\frac{20}{81} & \frac{56}{81} & \frac{1}{81} & \frac{4}{81} \\ \sqrt{N}\frac{8}{27} & \frac{2}{3} & 0 & \frac{1}{27} \end{pmatrix}.$$

We consider $\hat{M}_\nu, \nu = 1, \ldots, N-1$, and we compute the characteristic polynomial $p_\nu(\lambda)$ which turns out to be of the form

$$p_\nu(\lambda) = \frac{1}{2187}(27\lambda - 1)(81\lambda - 1)\left(\sum_{j=0}^{N-1} \beta_j \omega^{j\nu} - \lambda\right).$$

Thus, each block $\hat{M}_\nu, \nu = 1, \ldots, N-1$, has eigenvalues[1]

$$\lambda_0^\nu = \sum_{j=0}^{N-1} \beta_j \omega^{j\nu}, \quad \lambda_1^\nu = \frac{1}{27}, \quad \lambda_2^\nu = \frac{1}{81}. \tag{4.20}$$

In a similar way, we consider $\tilde{M}_0$ with characteristic polynomial

$$p_0(\lambda) = \frac{1}{2187}(\lambda - 1)(81\lambda - 1)(27\lambda - 1)(\alpha - \delta + \lambda),$$

and eigenvalues $\lambda_0^0 = 1$, $\lambda_1^0 = \delta - \alpha$, $\lambda_2^0 = \frac{1}{27}$, $\lambda_3^0 = \frac{1}{81}$. To find the admissible values of $\alpha, \beta_j, j = 0, \ldots, N-1$, and δ, imposing condition (i) in Table 1 we find

$$\delta - \alpha = \frac{1}{9}. \tag{4.21}$$

Remark 3 is still valid for the eigenvalues λ_0^ν in (4.20), so conditions (ii)-(iii) in Table 1 give rise to

$$\sum_{j=0}^{N-1} \beta_j \omega^j = \frac{1}{3}, \qquad \sum_{j=0}^{N-1} \beta_j \omega^{2j} = \frac{1}{9}. \tag{4.22}$$

Since λ_2^0, λ_3^0 and $\lambda_1^\nu, \lambda_2^\nu, \nu = 1, \ldots, N-1$, are equal to $\frac{1}{27}$ or $\frac{1}{81}$, to verify condition (iv) in Table 1, we only need to check that

$$\left| \sum_{j=0}^{N-1} \beta_j \omega^{j\nu} \right| \leq \frac{1}{9}, \qquad \text{for all } \nu = 3, \ldots, N-3.$$

[1]Note that for $N \geq 7$ the eigenvalue $\sum_{j=0}^{N-1} \beta_j \omega^{j\nu}$ could be smaller than $1/27$ for some ν, i.e. formally $\lambda_0^\nu < \lambda_1^\nu$, but, when the conditions in Table 1 are satisfied, the ordering of the remaining eigenvalues is not crucial. Since the general case $N > 7$ is not treated in detail, we decide to maintain such a notation.

Finally, since we require the convex hull property, all the coefficients found have to be in $[0,1]$.

Remark 5. *It is valid a consideration very similar to that in Remark 4. From (4.21) it is clear that α and δ are strictly related. If we find an expression for α, then $\delta = \frac{1}{9} + \alpha$ and, in order to ensure the convex hull property also for δ, we have to restrict the set of values for α to $\left[0, \frac{8}{9}\right]$. On the other hand, if we obtain δ, then $\alpha = \delta - \frac{1}{9}$ with $\delta \in \left[\frac{1}{9}, 1\right]$ for the convex hull property for α.*

In the following, we show the details of the computations for the special cases $N = 5, 7$.

Proposition 4.3. *Ternary Loop's scheme with extraordinary stencils in Figure 6 satisfies the conditions (I)-(IV) and the convex hull property at an extraordinary vertex of valence $N = 5$ if*

$$\beta_1 \in \left[\frac{2\sqrt{5}}{45}, \frac{7+\sqrt{5}}{45}\right] \approx [0.0994, 0.2052], \tag{4.23}$$

and

$$\alpha = \frac{7+\sqrt{5}}{9} - 5\beta_1, \quad \beta_0 = \beta_1 + \frac{10-\sqrt{5}}{45}, \quad \beta_2 = \beta_1 - \frac{2\sqrt{5}}{45}, \quad \delta = \frac{8+\sqrt{5}}{9} - 5\beta_1.$$

with $\beta_3 = \beta_2$ and $\beta_4 = \beta_1$.

Proof. We follow verbatim the proof of Proposition 4.1. The stencil weights involved in the subdivision rules in case of an extraordinary vertex of valence $N = 5$ are $\alpha, \beta_0, \beta_1, \beta_2$ and δ with

$$\beta_2 = \frac{1}{2}(1 - \alpha - \beta_0 - 2\beta_1). \tag{4.24}$$

Formulas (4.22) with (4.24) imply

$$\begin{aligned} \frac{1+\sqrt{5}}{4}\alpha + \frac{5+\sqrt{5}}{4}\beta_0 + \sqrt{5}\beta_1 - \frac{1+\sqrt{5}}{4} &= \frac{1}{3}, \\ \frac{1-\sqrt{5}}{4}\alpha + \frac{5-\sqrt{5}}{4}\beta_0 - \sqrt{5}\beta_1 - \frac{1-\sqrt{5}}{4} &= \frac{1}{9}, \end{aligned}$$

from which we compute

$$\alpha = \frac{7+\sqrt{5}}{9} - 5\beta_1, \qquad \beta_0 = \beta_1 + \frac{10-\sqrt{5}}{45},$$

and, as a consequence of (4.24), $\beta_2 = \beta_1 - \frac{2\sqrt{5}}{45}$. Moreover, (4.21) gives $\delta = \frac{8+\sqrt{5}}{9} - 5\beta_1$, and since for all $\nu = 0, \ldots, 4$ the remaining eigenvalues are equal to $\frac{1}{27}$ or $\frac{1}{81}$, condition (iv) in Table 1 is verified too. Now we have to ensure the convex hull property for all the parameters, that is, by considering Remark 5,

$$\begin{aligned} \alpha \in \left[0, \frac{8}{9}\right] \quad &\Leftrightarrow \quad \beta_1 \in \left[\frac{\sqrt{5}-1}{45}, \frac{7+\sqrt{5}}{45}\right] \approx [0.0275, 0.2052], \\ \beta_0 \in [0,1] \quad &\Leftrightarrow \quad \beta_1 \in \left[0, \frac{35+\sqrt{5}}{45}\right] \approx [0, 0.8275], \\ \beta_3 \in [0,1] \quad &\Leftrightarrow \quad \beta_1 \in \left[\frac{2\sqrt{5}}{45}, 1\right] \approx [0.0994, 1], \end{aligned}$$

and the intersection of these intervals (taking into account, if necessary, that also β_1 should be in $[0,1]$) gives (4.23). □

PROPOSITION 4.4. *Ternary Loop's scheme with extraordinary stencils in Figure 6 satisfies the conditions (I)-(IV) and the convex hull property at an extraordinary vertex of valence $N=7$ if, setting $c_j = 2\cos\frac{j\pi}{7}$, $j=2,4,6$,*

(4.25)
$$\beta_1 \in \left[\frac{2(4+c_2+c_4-2c_2c_6)}{9(7c_2+2c_4-9c_6+2c_2c_4-2c_4c_6)}, \frac{2(24+34c_2+11c_4-37c_6+6c_2c_4-13c_2c_6-7c_4c_6+2c_2c_4c_6)}{9(49c_2+5c_4-54c_6+5c_2c_4-5c_4c_6)}\right] \approx [0.0968, 0.2238],$$

(4.26)
$$\beta_2 \in \left[\max\left\{\frac{2+9(c_4-c_2)\beta_1}{9(c_4-c_6)}, 0, \frac{2(2c_2-c_4-c_6)}{9(c_2c_6+c_2c_4-6-c_4-c_6-c_2+c_4c_6)}+\beta_1\right\}, \min\left\{\frac{2(c_2-c_4)}{9(c_2c_6+c_2c_4-6-c_4-c_6-c_2+c_4c_6)}+\beta_1, \frac{4+6c_2-8c_6+9(2-4c_2+3c_4+2c_6-c_4c_6)\beta_1}{9(2+3c_2+2c_4-4c_6-c_2c_4)}\right\}\right],$$

and

$$\alpha = \frac{1}{9(c_2-c_6)}\left[4+6c_2-8c_6+9(2-4c_2+3c_4+2c_6-c_4c_6)\beta_1+ +9(-2-3c_2-2c_4+4c_6+c_2c_4)\beta_2\right], \tag{4.27}$$

$$\beta_0 = \frac{1}{9(c_2-c_6)}\left[3c_2-c_6+9(-2-c_4+c_4c_6)\beta_1+9(2+c_2-c_2c_4)\beta_2\right], \tag{4.28}$$

$$\beta_3 = \frac{1}{9(c_2-c_6)}\left[-2+9(c_2-c_4)\beta_1+9(c_4-c_6)\beta_2\right], \tag{4.29}$$

$$\delta = \frac{1}{9(c_2-c_6)}\left[4+7c_2-9c_6+9(2-4c_2+3c_4+2c_6-c_4c_6)\beta_1+ +9(-2-3c_2-2c_4+4c_6+c_2c_4)\beta_2\right], \tag{4.30}$$

with $\beta_4=\beta_3$, $\beta_5=\beta_2$ and $\beta_6=\beta_1$.

Proof. In case of an extraordinary vertex of valence $N=7$, the stencil weights are $\alpha, \beta_0, \beta_1, \beta_2, \beta_3$ and δ, with

$$\beta_3 = \frac{1}{2}\left(1-\alpha-\beta_0-2\beta_1-2\beta_2\right). \tag{4.31}$$

From (4.22) and (4.31), we have

$$\begin{aligned} -\frac{1}{2}c_6\alpha+\left(1-\frac{1}{2}c_6\right)\beta_0+(c_2-c_6)\beta_1+(c_4-c_6)\beta_2+\frac{1}{2}c_6 &= \frac{1}{3},\\ -\frac{1}{2}c_2\alpha+\left(1-\frac{1}{2}c_2\right)\beta_0+(c_4-c_2)\beta_1+(c_6-c_2)\beta_2+\frac{1}{2}c_2 &= \frac{1}{9}. \end{aligned}$$

These equations give α and β_0 as in (4.27)-(4.28), and we obtain β_3 and δ in (4.29)-(4.30) as a consequence of (4.31) and (4.21), respectively. Moreover, to verify also condition (iv) in Table 1, we need to check if all the other eigenvalues are not greater than $\frac{1}{9}$. Since λ_2^0, λ_3^0 and $\lambda_1^\nu, \lambda_2^\nu, \nu=1,\dots,6$, are equal to $\frac{1}{27}$ or $\frac{1}{81}$, we have just to check if $|\lambda_0^3|, |\lambda_0^4| \le \frac{1}{9}$. Since Remark 3 ensures that $\lambda_0^3=\lambda_0^4$, the previous inequality

is verified from (4.20) with $\nu = 3$ if

$$-\frac{1}{9} \leq \frac{9(c_2c_6 + c_2c_4 - 6 - c_4 - c_6 + c_4c_6 - c_2)(\beta_1 - \beta_2) + 3c_2 - c_6 - 2c_4}{9(c_2 - c_6)} \leq \frac{1}{9},$$

that is

$$\lambda_0^3 \in \left[-\frac{1}{9}, \frac{1}{9}\right] \quad \Leftrightarrow \quad \beta_2 \in \frac{[4c_2 - 2c_4 - 2c_6, 2c_2 - 2c_4]}{9(c_2c_6 + c_2c_4 - 6 - c_4 - c_6 - c_2 + c_4c_6)} + \beta_1. \tag{4.32}$$

Now we check the convex hull property, by remembering Remark 5,

$$\begin{aligned}
&\alpha \in \left[0, \frac{8}{9}\right] \quad \Leftrightarrow \quad \beta_2 \in \frac{[4 - 2c_2, 4 + 6c_2 - 8c_6] + 9(2 - 4c_2 + 3c_4 + 2c_6 - c_4c_6)\beta_1}{9(2 + 3c_2 + 2c_4 - 4c_6 - c_2c_4)}, \\
&\beta_0 \in [0, 1] \quad \Leftrightarrow \quad \beta_2 \in \frac{[3c_2 - c_6, -6c_2 + 8c_6] + 9(-2 - c_4 + c_4c_6)\beta_1}{9(c_2c_4 - 2 - c_2)}, \\
&\beta_3 \in [0, 1] \quad \Leftrightarrow \quad \beta_2 \in \frac{[2, 2 + 9c_2 - 9c_6] + 9(c_4 - c_2)\beta_1}{9(c_4 - c_6)}.
\end{aligned} \tag{4.33}$$

We observe that all the eligible values for β_2 in (4.33) and (4.32), for $\beta_1 \in [0, 1]$, are contained in regions of the plane delimited by two parallel lines (see Figure 7). The intersection of such regions, taking into account that also β_2 should be in $[0, 1]$ and using the notation explained in the caption of Figure 7, gives rise to

$$\begin{aligned}
&\beta_1 \in [(\beta_3)_{\mathrm{L}} \cap (\lambda_0^3)_{\mathrm{R}}, (\lambda_0^3)_{\mathrm{L}} \cap (\alpha)_{\mathrm{R}}], \\
&\beta_2 \in [\max\{(\beta_3)_{\mathrm{L}}, 0, (\lambda_0^3)_{\mathrm{L}}\}, \min\{(\lambda_0^3)_{\mathrm{R}}, (\alpha)_{\mathrm{R}}\}],
\end{aligned}$$

which are written in full in (4.25) and (4.26). □

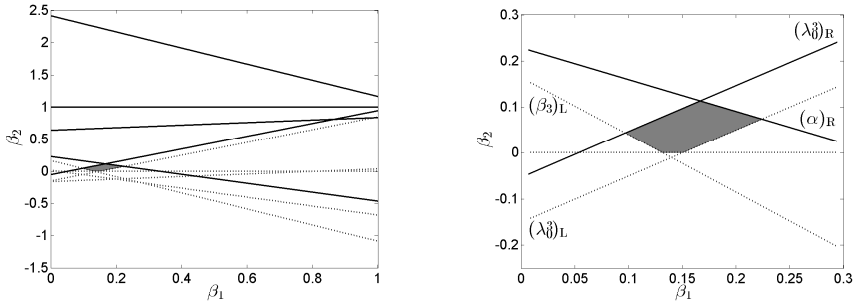

(a) (b)

Fig. 7. (a): $(\cdots)$ *lines demarcating the eligible regions from left,* $(-)$ *lines demarcating the eligible regions from right for* β_2*, given in (4.33) and (4.32), with* $\beta_1 \in [0, 1]$*: in gray is depicted the intersection of such eligible regions.* (b) *Zoom of the eligibility region in* (a) *with indications about the involved lines:* $(\theta)_{\mathrm{L}}$ *and* $(\theta)_{\mathrm{R}}$ *are, respectively, the left and the right demarcating lines of the regions of values for* β_2 *related to* $\theta \in \{\alpha, \beta_3, \lambda_0^3\}$*.*

5. Conclusions. To determine the ranges of variability of the extraordinary stencil weights of a primal surface subdivision scheme, we have proposed an efficient computational approach based on the spectral analysis of the hybrid block-circulant

matrix incorporating the subdivision rules. The usefulness of our strategy has been shown on two examples of subdivision schemes for triangular meshes: a binary 1-ring scheme and a ternary 2-ring scheme, which both improve original Loop's algorithm. In particular, for such schemes we compute the ranges in which the free parameters could vary in order to satisfy the spectral conditions needed to obtain C^1 limit surfaces with bounded curvature, convex hull property and optimal shrinkage in case of extraordinary vertices of valence $N = 5$ and $N = 7$. As pointed out by some recent research on triangle meshes, such valences are indeed the only ones of primary importance, since any triangular mesh containing extraordinary vertices of any valence can be transformed into a 567-mesh capable of representing the same surface of arbitrary manifold topology.

Acknowledgement. The work of the first three authors and of the last author is supported in part by MIUR - PRIN 2012 N. 2012MTE38N and by grants of the group GNCS of INdAM.

REFERENCES

[1] N. Aghdaii, H. Younesy, H. Zhang, 5-6-7 Meshes: remeshing and analysis, Comput. Graph. 36(8), 1072-1083 (2012).
[2] A.A. Ball, D.J.T. Storry, A matrix approach to the analysis of recursively generated B-spline surfaces, Computer-Aided Design 18(10), 437-442 (1986).
[3] L. Barthe, L. Kobbelt, Subdivision scheme tuning around extraordinary vertices, Comput. Aided Geom. Design 21(6), 561-583 (2004).
[4] D.A. Bini, G. Latouche, B. Meini, Numerical methods for structured Markov chains. Numerical Mathematics and Scientific Computation. Oxford Science Publ.. Oxford Univ. Press, New York, 2005
[5] P. Davis, Circulant Matrices, J. Wiley and Sons, New York, 1979.
[6] V. Del Prete, F. Di Benedetto, M. Donatelli, S. Serra-Capizzano, Symbol approach in a signal-restoration problem involving block Toeplitz matrices, J. Comput. Appl. Math. 272, 399-416 (2014).
[7] D. Doo, M.A. Sabin, Behaviour of Recursive Subdivision Surfaces Near Extraordinary Points, Computer-Aided Design 10(6), 189194 (1978).
[8] A. Dorostkar, M. Neytcheva, S. Serra-Capizzano, Spectral analysis of coupled PDEs and of their Schur complements via the notion of Generalized Locally Toeplitz sequences, in revision for Comput. Meth. Appl. Mech. Eng.. Technical Report, N. 8, January 2015, Department of Information Technology, Uppsala University.
[9] C. Garoni, S. Serra-Capizzano, D. Sesana, Spectral analysis and spectral symbol of d-variate $\mathbf{Q}_p$ Lagrangian FEM stiffness matrices, SIAM J. Matrix Anal.Appl., 36(3), 1100-1128 (2015).
[10] I. Ginkel, G. Umlauf, Loop subdivision with curvature control, Eurographics Symposium on Geometry Processing (2006).
[11] X.Q. Jin, Developments and applications of block Toeplitz iterative solvers. Combinatorics and Computer Science, 2. Kluwer Acad. Publ. Group, Dordrecht; Science Press Beijing, Beijing, 2002.
[12] C. Loop, Smooth Subdivision Surfaces Based on Triangles. M.S. Mathematics thesis, 1987. University of Utah.
[13] C. Loop, Bounded curvature triangle mesh subdivision with the convex hull property, The Visual Computer 18, 316–325 (2002).
[14] C. Loop, Smooth ternary subdivision of triangle meshes, Curve and Surface Fitting: Saint-Malo 2002, A. Cohen, J.L. Merrien and L.L. Schumaker (eds), Nashboro Press, Brentwood, pages 295-302 (2003).
[15] J. Peters, U. Reif, Subdivision Surfaces, Springer, 2008.
[16] J. Peters, U. Reif, Shape characterization of subdivision surfaces - basic principles, Comput. Aided Geom. Design 21(6), 585–599 (2004).
[17] U. Reif, A unified approach to subdivision algorithms near extraordinary vertices, Comput. Aided Geom. Design 12, 153-174 (1995).
[18] M.A. Sabin, L. Barthe, Artifacts in recursive subdivision surfaces, Curve and Surface Fit-

ting: Saint-Malo 2002, A. Cohen, J.L. Merrien and L.L. Schumaker (eds), Nashboro Press, Brentwood, pages 353-362 (2003).
[19] J. Stam, Exact evaluation of Catmull-Clark subdivision surfaces at arbitrary parameter values, In SIGGRAPH 98: Proceedings of the 25th annual conference on Computer graphics and interactive techniques (New York, NY , USA, 1998), ACM Press, pages 395-404 (1998).
[20] V. Vidal, G. Lavoue, F. Dupont, Low budget and high fidelity relaxed 567-remeshing, Comput. Graph. 47, 16-23 (2015).
[21] D. Zorin, Stationary subdivision and multiresolution surface representations. PhD thesis, 1997. Caltech, Pasadena, California.
[22] D. Zorin, A method for analysis of C^1-continuity of subdivision surfaces. SIAM J. Numer. Anal. 35(5), 1677-1708 (2000).